Plasmonics (2013) 8:797–801
DOI 10.1007/s11468-012-9475-9

Fano Resonance in a Gear-Shaped Nanocavity of the Metal–Insulator–Metal Waveguide

Z.-D. Zhang · H.-Y. Wang · Z.-Y. Zhang

Received: 29 August 2012 / Accepted: 3 December 2012 / Published online: 13 December 2012

Abstract The filter function of the metal–insulator–metal (MIM) waveguide with a gear-shaped nanocavity is investigated using the finite-difference time-domain method. Since the gear breaks the symmetric distribution of the resonance, Fano resonance occurs in the gear-shaped nanocavity. Fano resonance strongly depends on the structural parameters of the gear. Compared to the MIM waveguide with a disk-shaped nanocavity, the MIM waveguide with a gear-shaped nanocavity allows for a much more sensitive detection of small refractive index changes of the filled media inside the nanocavity, which reveals a potential sensor application of the MIM waveguide with a gear-shaped nanocavity.

Keywords Surface plasmon polariton · Fano resonance · Gear-shaped nanocavity · Finite-difference time-domain method

Introduction

Surface plasmon polaritons (SPPs) are electromagnetic waves formed by the interference between the photon and the electron at the surface of a metal film [1]. SPPs have raised tremendous interest on emerging applications, including waveguides [2], magneto-optic data storages [3], solar cells [4], and sensors [5]. For the waveguide application, two basic types of SPP waveguides, insulator–metal–insulator waveguide [6, 7] and metal–insulator–metal (MIM) waveguide [8–10], are widely investigated. Since MIM waveguide has a small mode size, MIM waveguides are paid more attention, and photonic devices based on the MIM waveguide, such as filters [8, 9], splitters [10], and couplers [11], have been realized. The resonant wavelengths of the filter based on MIM waveguide strongly depend on the refractive index of the filled media inside the nanocavity. Thus, the filter enables the detection of the refractive index changes [9]. This kind of sensor is a lab on a chip, and its potential application is tremendous. By optimizing the topological shape of the nanocavity of the MIM waveguide, the sensitivity of the sensor for the refractive index could be largely improved. One possible scheme is to achieve Fano resonance in the nanocavity.

Fano resonance arises directly from the constructive and the destructive interference of a narrow discrete resonance with a broad spectral line or continuum [12, 13]. As an interference phenomenon, Fano resonance is coherent sensitive to the changes of the geometry and local dielectric environment. A small perturbation can induce dramatic resonance or line shape shift [13–16], which enables the fabrication of ultra-sensitive sensors based on Fano resonance. Researchers have designed different Fano resonance systems based on the localized surface plasmon resonance (LSPR), such as dolmen nanostructure [17], cluster of nanospheres [18], nanodisk with a missing wedge-shaped slice [19], non-concentric ring/disk cavity [14], and nanocube on a semi-infinite dielectric base layer [13]. Fano resonance based on LSPR has achieved ultra-sensitivity to the refractive index of the surrounding media. However, Fano resonance based on SPPs in the plasmonic waveguide is less studied. We hypothesize that Fano resonance based on SPPs could show ultra-sensitivity to the refractive index of the filled media inside the nanocavity, similar to that based on LSPR.

In this paper, a gear-shaped nanocavity is proposed to produce Fano resonance, and the transmission properties of the MIM waveguide with a gear-shaped nanocavity are investigated

Z.-D. Zhang · Z.-Y. Zhang (✉)
College of Physics and Information Technology, Shaanxi Normal University, Xi'an 710062, China
e-mail: zyzhang@snnu.edu.cn

Z.-D. Zhang · H.-Y. Wang
School of Physical Science and Technology, Southwest Jiaotong University, Chengdu 610031, China

using the finite-difference time-domain (FDTD) method and compared with those of the MIM waveguide with a disk-shaped nanocavity. Since the gear breaks the symmetric distribution of the resonant modes of the disk-shaped nanocavity, Fano resonance occurs in the gear-shaped nanocavity. The structural parameter effects on the Fano resonance are investigated. In addition, the sensitivities of the resonant modes to the refractive index of the filled media inside the gear-shaped nanocavity are studied and compared with those of the disk-shaped nanocavity. It is shown that the gear-shaped nanocavity allows a much more sensitive detection of the refractive index changes when Fano resonance occurs in the nanocavity.

Structure and Computational Methods

Figure 1 shows the MIM waveguide with a gear-shaped nanocavity. The width w of the MIM waveguide is fixed at 50 nm to ensure that only the fundamental transverse magnetic (TM_0) mode is supported [20, 21]. d is the distance between the gear-shaped nanocavity and the MIM waveguide. The central angle of the teeth of the gear is θ. The radius of the dedendum circle is fixed at R=300 nm. r is the radius of the addendum circle. Therefore, the teeth of the gear have the height $h=R-r$. For all calculations, the lateral surface of the teeth close to the waveguide is perpendicular to the waveguide (along the y direction in Fig. 1). The thickness (in z direction) of the structure is fixed at 600 nm.

The transmission properties of the MIM waveguide with a gear-shaped nanocavity are simulated using a commercial FDTD software (XFDTD by Remcom Inc.). The frequency-dependent complex relative permittivity $\varepsilon(\omega)$ of silver is characterized by the modified Debye mode [22]. A dipole source S in the middle of the waveguide at a distance of 550 nm away from the center of the gear-shaped nanocavity oscillates as a Gaussian pulse along the y direction to excite the TM_0 mode in the MIM waveguide. The transmittance is determined as $T=P_T/P_0$, where P_T is the transmitted energy flow in the MIM waveguide with a gear-shaped nanocavity and P_0 is the transmitted energy flow in the MIM waveguide without the gear-shaped nanocavity. The transmitted energy flow is determined by integrating the x component of the Poynting vector over the cross section of the port P at a distance of 1,000 nm from the dipole source.

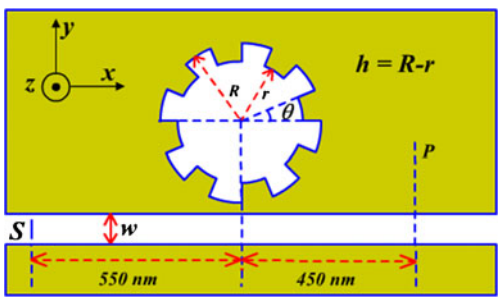

Fig. 1 (Color online) Schematics for the MIM waveguide with a gear-shaped nanocavity and the dipole excitation

Results and Discussion

Figure 2a shows the transmission spectrum of the MIM waveguide with the gear-shaped nanocavity of r=260 nm, $h=R-r$=40 nm, and $\theta=\pi/12$. Six resonant modes (G_0, G_1, G_2, G_3, G_4, and G_5) appear in the transmission spectrum. For comparison, the transmission spectrum of the MIM waveguide with a disk-shaped nanocavity is also calculated. The radius of the disk-shaped nanocavity is the same as the radius of the dedendum circle of the gear-shaped nanocavity, which is 300 nm. As shown in Fig. 2b, five resonant modes (D_0, D_1, D_2, D_3, and D_4) appear in the transmission spectrum of the MIM waveguide with the disk-shaped nanocavity.

To determine the origins of the resonant modes of the gear-shaped nanocavity, the normalized $|H_z|$ field distributions of the gear-shaped nanocavity at resonant wavelengths are calculated and compared with those of the disk-shaped nanocavity. Subpanels a to d of Fig. 3 show the normalized $|H_z|$ field distributions of the disk-shaped nanocavity at resonant wavelengths of λ_{D0}=1.146 μm, λ_{D1}=0.712 μm, λ_{D2}=0.54 μm, and λ_{D3}=0.45 μm, respectively. The standing waves are formed inside the nanocavity. The mode numbers of D_0, D_1, D_2, and D_3 are 1, 2, 3, and 4, respectively. We also calculated the normalized $|H_z|$ field distribution at λ_{D4}=0.42 μm, and the mode number is 5 (data not shown). For the MIM waveguide with the gear-shaped nanocavity, at λ_{G0}=1.153 μm, as shown in Fig. 3e, the mode number is 1, and there is a similar $|H_z|$ field distribution as Fig. 3a, which denotes the same resonant mode of

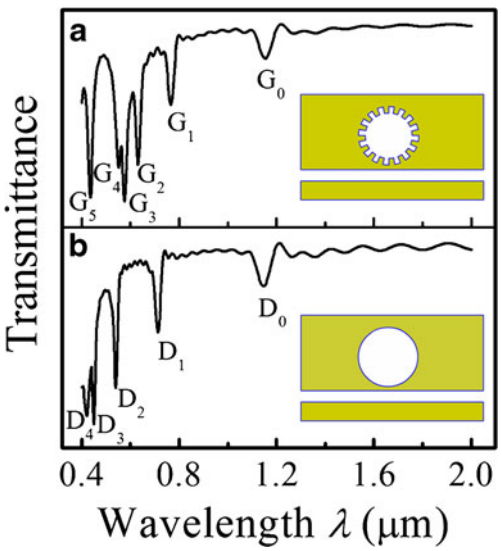

Fig. 2 (Color online) Transmission spectra of the MIM waveguide with different nanocavities: **a** the gear-shaped nanocavity, **b** the disk-shaped nanocavity

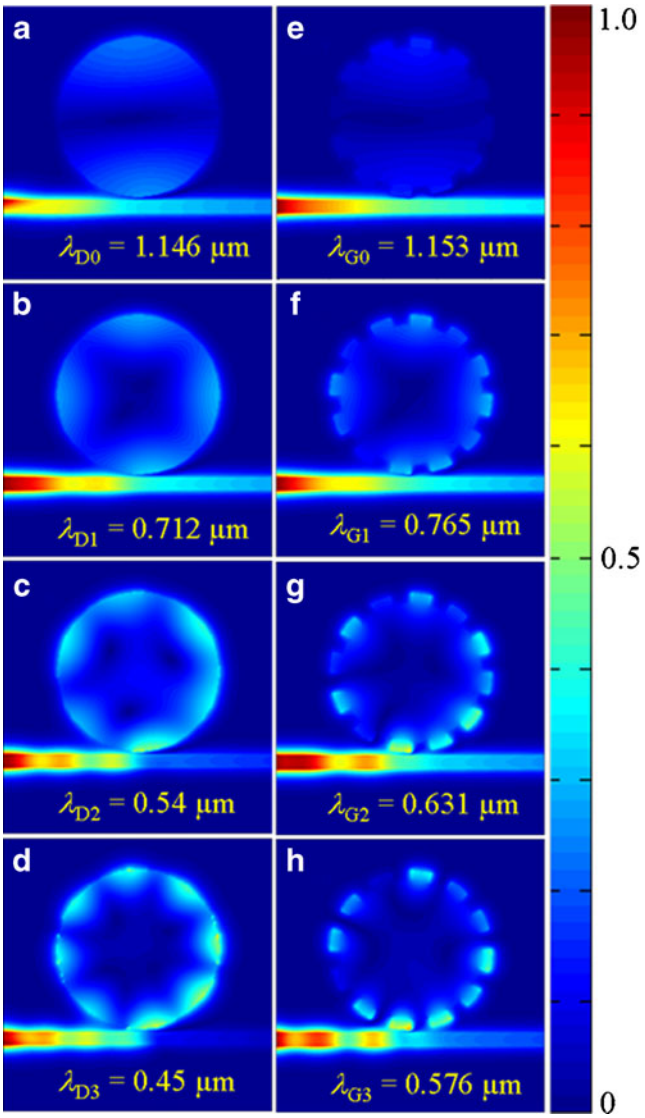

Fig. 3 (Color online) Contour profiles of the normalized $|H_z|$ fields of the MIM waveguide with different nanocavities at different wavelengths: **a–d** the disk-shaped nanocavity, **e–h** the gear-shaped nanocavity

the disk-shaped nanocavity at λ_{D0}=1.146 μm. At λ_{G1}= 0.765 μm, as shown in Fig. 3f, the mode number is 2, and there is a similar $|H_z|$ field distribution as Fig. 3b, which denotes the same resonant mode of the disk-shaped nanocavity at λ_{D1}=0.712 μm. At λ_{G2}=0.631 μm, as shown in Fig. 3g, large $|H_z|$ fields distribute in the spaces between adjacent teeth, and it is hard to distinguish the mode number. Similarly, at λ_{G3}=0.576 μm (Fig. 3h), λ_{G4}=0.552 μm, and λ_{G5}=0.436 μm, it is also hard to distinguish the mode number in the gear-shaped nanocavity. For the gear-shaped nanocavity, at smaller resonant wavelengths, the teeth break the symmetry of the $|H_z|$ field distribution, and more complicated resonant modes occur in the transmission spectrum. This can be explained by the Fano resonance from the interference between the discrete resonance of adjacent teeth and the symmetric distribution of the resonance in the nanocavity.

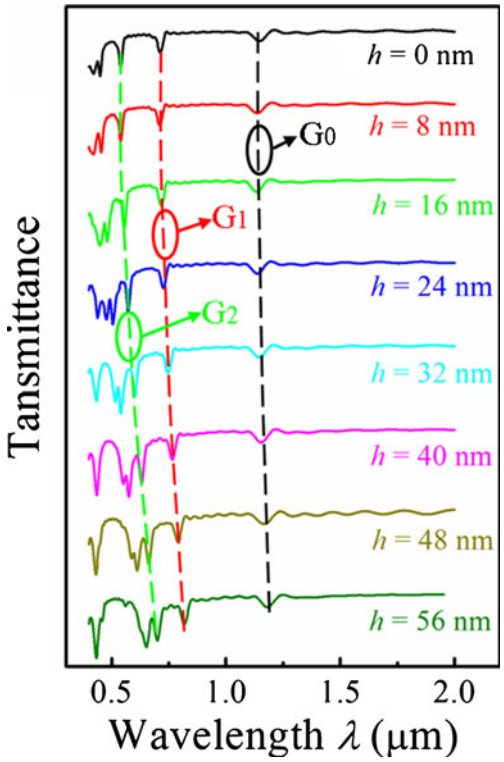

Fig. 4 (Color online) Transmission spectra of the MIM waveguide with the gear-shaped nanocavities with different teeth height h

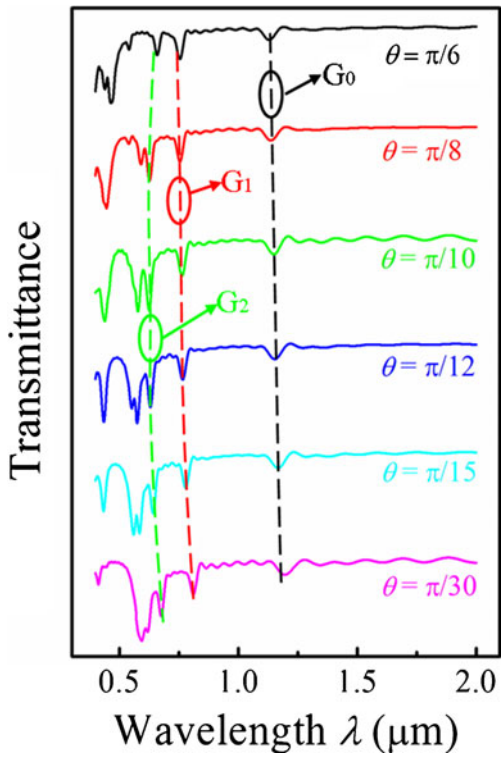

Fig. 5 (Color online) Transmission spectra of the MIM waveguide with the gear-shaped nanocavities with different central angle θ

To investigate the effect of the teeth height h on the Fano resonance in the gear-shaped nanocavity, h is increased from h=0 nm to h=56 nm at fixed $\theta=\pi/12$. As shown in Fig. 4, G_0 mode is weakly affected by h. However, with increased h, the wavelengths of G_1, G_2, and G_3 modes red-shift. At the same time, the transmission spectra become more complex. There are five resonant modes when h is increased from h=0 nm to h=16 nm. When h is increased from h=24 nm to h=48 nm, there are six resonant modes. However, when h reaches h=56 nm, one resonant mode disappears, and the mode number decreases to 5. For smaller h, the resonant modes are weakly affected by the teeth. With increased h, the LSPR between adjacent teeth break the symmetric distribution of the $|H_z|$ field, which results in the complicated transmission spectrum. However, for larger h, the SPPs propagate at the top of the teeth, and the LSPR between adjacent teeth are relatively weak. Thus, the interactions between them are also relatively weak, which results in the similar transmission spectra for smaller h and larger h. Fano resonance only occurs in the gear-shaped nanocavity, when h has appropriate value.

In order to investigate how θ influences the Fano resonance, θ is decreased from $\theta=\pi/6$ to $\theta=\pi/30$ at fixed h=40 nm. As shown in Fig. 5, when $\theta=\pi/6$, there are five resonant modes at 1.13, 0.754, 0.66, 0.466, and 0.439 μm, respectively. When θ decreases to $\theta=\pi/8$, one resonant mode appears at λ_{G3}=0.59 μm, and the resonant mode at the blue side of the dip of 0.466 μm disappears. For $\theta=\pi/10$, there are similar resonant modes as those of $\theta=\pi/8$. When θ decreases to $\theta=\pi/12$, a new resonant mode appears at λ_{G4}=0.552 μm. With further decrease of θ, there is no new resonant mode. Since the distribution of the teeth depends on θ, the distribution of LSPR between adjacent teeth also depends on θ. The θ-dependent interaction between LSPR and the symmetric distribution of the resonance in the nanocavity results in the strongly θ-dependent resonant modes in Fig. 5.

To show that the teeth contribute to the sensitivity of the resonant modes, we compare the sensitivities to the refractive index of the filled media inside the nanocavity between the resonant modes of the MIM waveguide with the disk-shaped nanocavity and those of the gear-shaped nanocavity. The two types of nanocavity have the same structural parameters as

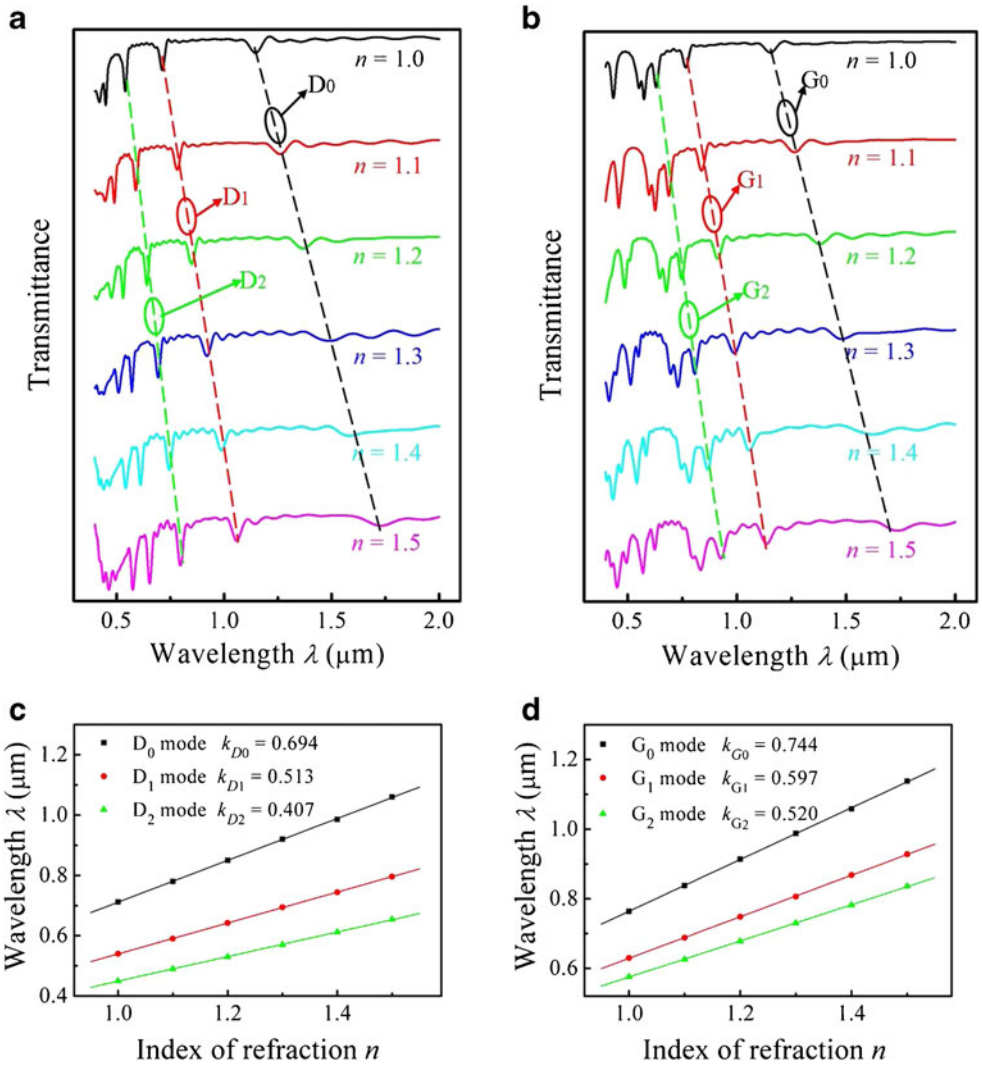

Fig. 6 (Color online) **a**, **b** Transmission spectra of the MIM waveguide with the disk-shaped nanocavity (**a**) and the MIM waveguide with the gear-shaped nanocavity (**b**) filled by different refractive index n. **c**, **d** Resonant wavelengths of the MIM waveguide with the disk-shaped nanocavity (**c**) and the MIM waveguide with the gear-shaped nanocavity (**d**) as a function of the refractive index n

those in Fig. 2. Subpanels a and b of Fig. 6 show the transmission spectra of the disk-shaped nanocavity and the gear-shaped nanocavity with different filled refractive index n, respectively. For two types of nanocavity, with increased n, the wavelengths of the resonant modes red-shift, and new resonant modes appear at the blue side of the transmission spectra. Figure 6c shows the wavelength of the resonant modes D_0, D_1, and D_2 as a function of n. The solid curves are the linear fittings. The slopes of them are k_{D0}=0.694, k_{D1}=0.513, and k_{D2}=0.407, respectively. Figure 6d shows the wavelengths of G_0, G_1, and G_2 as a function of n. The solid curves are also the linear fittings. The slopes of them are k_{G0}=0.744, k_{G1}=0.597, and k_{G2}=0.520, respectively. For the similar resonant modes D_0/G_0 and D_1/G_1, the differences of the slopes between them are 0.05 and 0.084, respectively. However, when Fano resonance occurs in the gear-shaped nanocavity (G_2 mode), the difference of the slope between D_2 and G_2 is 0.113, which is much larger than those of D_0/G_0 and D_1/G_1. Therefore, when Fano resonance occurs in the gear-shaped nanocavity, the resonant wavelength is more sensitive to the refractive index, which enables a sensitive way to detect the changes of the refractive index.

Conclusion

In this paper, the transmission properties of the MIM waveguide with a gear-shaped nanocavity are investigated numerically and compared with those of the MIM waveguide with a disk-shaped nanocavity. Since the LSPR between adjacent teeth breaks the symmetric distribution of the resonance of the disk-shaped nanocavity, Fano resonance occurs in the gear-shaped nanocavity. Fano resonance strongly depends on the height and the central angle of the teeth. In addition, Fano resonance is more sensitive to the refractive index changes of the filled media inside the nanocavity, which provides a novel way of building plasmonic sensors based on SPP waveguides for the detection of refractive index changes.

Acknowledgments The work was supported by the National Natural Foundation of China (grant nos. 11004160 and 10974161) and the Innovation Fund for Ph.D. students of Southwest Jiaotong University.

References

1. Raether H (1988) Surface plasmons on smooth and rough surfaces and gratings. Springer, Berlin
2. Gramotnev DK, Bozhevolnyi SI (2010) Plasmonics beyond the diffraction limit. Nat Photonics 4:83–91. doi:10.1038/nphoton.2009.282
3. Bonod N, Reinisch R, Popov E, Nevière M (2004) Optimization of surface-plasmon-enhanced magneto-optical effects. J Opt Soc Am B 21:791–797. doi:10.1364/JOSAB.21.000791
4. Derkacs D, Lim SH, Matheu P, Mar W, Yu ET (2006) Improved performance of amorphous silicon solar cells via scattering from surface plasmon polaritons in nearby metallic nanoparticles. Appl Phys Lett 89:093103–093105. doi:10.1063/1.2336629
5. Charbonneau R, Tencer M, Lahoud N, Berini P (2008) Demonstration of surface sensing using long-range surface plasmon waveguides on silica. Sens Actuators B: Chem 134:455–461. doi:10.1016/j.snb.2008.05.034
6. Rosenzveig T, Hermannsson PG, Leosson K (2010) Modeling of polarization-dependent loss in plasmonic nanowire waveguides. Plasmonics 5:75–77. doi:10.1007/s11468-009-9118-y
7. Fang YR, Li ZP, Huang YZ, Zhang SP, Nordlander P, Halas NJ, Xu HX (2010) Branched silver nanowires as controllable plasmon routers. Nano Lett 10:1950–1954. doi:10.1021/nl101168u
8. Zhang ZY, Wang JD, Zhao YN, Lu D, Xiong ZH (2011) Numerical investigation of a branch-shaped filter based on metal-insulator-metal waveguide. Plasmonics 6:773–778. doi:10.1007/s11468-011-9263-y
9. Jin XP, Huang XG, Tao J, Lin XS, Zhang Q (2010) A novel nanometeric plasmonic refractive index sensor. IEEE T Nanotechnol 9:134–137. doi:10.1109/TNANO.2009.2038909
10. Veronis G, Fan S (2005) Bends and splitters in metal-dielectric-metal subwavelength plasmonic waveguides. Appl Phys Lett 87:131102–131104. doi:10.1063/1.2056594
11. Nikolajsen T, Leosson K, Bozhevolnyi SI (2004) Surface plasmon polariton based modulators and switches operating at telecom wavelengths. Appl Phys Lett 85:5833–5835. doi:10.1063/1.1835997
12. Luk'yanchuk B, Zheludev NI, Maier SA, Halas NJ, Nordlander P, Giessen H, Chong CT (2010) The Fano resonance in plasmonic nanostructures and metamaterials. Nat Mater 9:707–715. doi:10.1038/nmat2810
13. Zhang SP, Bao K, Halas NJ, Xu HX, Nordlander P (2011) Substrate-induced Fano resonances of a plasmonic nanocube: a route to increased-sensitivity localized surface plasmon resonance sensors revealed. Nano Lett 11:1657–1663. doi:10.1021/nl200135r
14. Hao F, Sonnefraud Y, Van Dorpe P, Maier SA, Halas NJ, Nordlander P (2008) Symmetry breaking in plasmonic nanocavities: subradiant LSPR sensing and a tunable Fano resonance. Nano Lett 8:3983–3988. doi:10.1021/nl802509r
15. Spinelli P, van Lare C, Verhagen E, Polman A (2011) Controlling Fano lineshapes in plasmon-mediated light coupling into a substrate. Opt Express 19:A303–A311. doi:10.1364/OE.19.00A303
16. Tam F, Moran C, Halas N (2004) Geometrical parameters controlling sensitivity of nanoshell Plasmon resonances to changes in dielectric environment. J Phys Chem B 108:17290–17294. doi:10.1021/jp048499x
17. Verellen N, Sonnefraud Y, Sobhani H, Hao F, Moshchalkov VV, Dorpe PV, Nordlander P, Maier SA (2009) Fano resonances in individual coherent plasmonic nanocavities. Nano Lett 9:1663–1667. doi:10.1021/nl9001876
18. Lassiter JB, Sobhani H, Fan JA, Kundu J, Capasso F, Nordlander P, Halas NJ (2010) Fano resonances in plasmonic nanoclusters: geometrical and chemical tunability. Nano Lett 10:3184–3189. doi:10.1021/nl102108u
19. Fang ZY, Cai JY, Yan ZB, Nordlander P, Halas NJ, Zhu X (2011) Removing a wedge from a metallic nanodisk reveals a Fano resonance. Nano Lett 11:4475–4479. doi:10.1021/nl202804y
20. Kekatpure RD, Hryciw AC, Barnard ES, Brongersma ML (2009) Solving dielectric and plasmonic waveguide dispersion relations on a pocket calculator. Opt Express 17:24112–24129. doi:10.1364/OE.17.024112
21. Yun BF, Hu GH, Cui YP (2010) Theoretical analysis of a nanoscale plasmonic filter based on a rectangular metal-insulator-metal waveguide. J Phys D Appl Phys 43:35102–35109. doi:10.1088/0022-3727/43/38/385102
22. Gai H, Wang J, Tian Q (2007) Modified Debye model parameters of metals applicable for broadband calculations. Appl Opt 46:2229–2233. doi:10.1364/AO.46.002229